Preferential alkali metal adduct formation by *cis* geometrical isomers of dicaffeoylquinic acids allows for efficient discrimination from their *trans* isomers during UHPLC-QTOF-MS.

Mpho M. Makola[a], Paul. A Steenkamp[a,b], Ian A. Dubery[a], Mwadham M. Kabanda[c], Ntakadzeni E. Madala[a*]

[a] Department of Biochemistry, University of Johannesburg, P.O. Box 524, Auckland Park 2006, South Africa

[b] CSIR Biosciences, Natural Products and Agroprocessing Group, Pretoria, 0001, South Africa

[c] Department of Chemistry, North-West University (Mafikeng Campus), Private Bag x2046, Mmabatho 2735, South Africa

Corresponding author: NE Madala; Tel: +2711 559 4573; Fax: +2711 559 2605; email: emadala@uj.ac.za

ABSTRACT

RATIONALE: Caffeoylquinic acid (CQA) derivatives are a group of structurally diverse phytochemicals that have attracted attention due to their many health benefits. The structural diversity of these molecules is due in part to the presence of regio- and geometrical isomerism. This structural diversity hampers the accurate annotation of these molecules in plant extracts. Mass spectrometry (MS) is successfully used to differentiate between the different regioisomers of the CQA derivatives; however, the accurate discrimination of the geometrical isomers of these molecules has proven to be an elusive task.

METHODS: UV-irradiated methanolic solutions of diCQA were analysed using an UHPLC-QTOF-MS method in negative ionisation mode. An in-source collision induced dissociation (ISCID) method was optimized by varying both the capillary and cone voltages to achieve differential fragmentation patterns between UV-generated geometrical isomers of the diCQAs during MS analyses.

RESULTS: Changes in the capillary voltage did not cause a significant difference to the fragmentation patterns of the four geometrical isomers, while changes in the cone voltage resulted in significant differences in the fragmentation patterns. The results also show, for the first time, the preferential formation of alkali metal (Li^+, Na^+ and K^+) adducts by the *cis* geometrical isomers of diCQAs, compared to their *trans* counterparts.

CONCLUSION: Optimised QTOF-MS based methods may be used to differentiate the geometrical isomers of diCQAs. Finally, additives such as metal salts to induce adduct formation can be applied as an alternative method to differentiate closely related isomers which could have been difficult to differentiate under normal MS settings.

Keywords: Chlorogenic acids, geometrical isomers, fragmentation, sodium adduct, QTOF-MS, Cone voltage.

INTRODUCTION

Caffeoylquinic acid (CQA) derivatives, members of the chlorogenic acid (CGA) family of plant polyphenolics, are widely occurring in plants and have been the subject of interest for decades due to their assumed health benefits. [1,2] These phytochemicals are amongst the most ubiquitous polyphenolic compounds in plants and are constituents of most food and medicinal plants. [1,3,4] The interest in these molecules lies in their health benefits which include anti-oxidant [5], anti-HIV1 [6] and anti-inflammatory [7] activities. The *cis-trans* isomerisation of these molecules as a result of UV irradiation of natural plant material and authentic standards has been reported elsewhere. [8-10] These *cis-trans* photo-isomerization reactions combined with the natural occurrence of positional (regio-) isomers add to the structural diversity of these phytochemicals and it is this diversity that poses an undisputed analytical challenge that hampers the accurate identification and quantification of these molecules in plant extracts. [8, 10] The development of accurate techniques for the annotation of these molecules is, therefore, of importance due to the growth in the field of ethno-pharmacology where various teas and herbal extracts are marketed for their health benefits which are dependent on the presence and abundance of molecules such as CQA derivatives.[11]

Analytical techniques such as nuclear magnetic resonance (NMR) spectroscopy have been used to distinguish between various regio- and geometrical (*cis-trans*) isomers of some natural products.[12] However, challenges due to signal overlapping and inadequate sensitivity associated with this technique have led to the wider application of mass spectrometric analyses in plant studies. [13-15] Mass spectrometry (MS) is not only selective and sensitive but can also be interfaced with gas chromatography (GC) [16] and liquid chromatography (LC) [17] separation instruments with relative ease. Liquid chromatography coupled with mass spectrometry (LC-MS) has been the method of choice for the analyses of plant extracts, especially CGA analyses. [3,18-19] In the analyses of CQA and other CGAs, ion-trap mass spectrometry (IT-MS) has been successfully used to discriminate between the different classes of CGAs, resulting in the development of hierarchical keys that can be used to unambiguously distinguish between the various regioisomers thereof. [3,8,18-20] However, IT-MS based techniques have not been able to distinguish between the geometrical isomers of the mono- and di-CQA. [8, 20] Increasingly, other mass spectrometry methods such as quadrupole-time of flight (Q-TOF) MS are being used for the analyses of plant extracts. [9,13,21] Recently, Madala et al. [22] developed and optimised an in source collision induced

dissociation (ISCID) UPLC-QTOF-MS based method to distinguish between the *cis* and *trans* isomers of 4-acylated CGAs in three *Momordica* plant species. This ability of ISCID-based QTOF-MS methods over the multistage fragmentation approach on the IT-MS to distinguish between the *cis* and *trans* isomers of 4-CQA, may possibly be due to the fact that unlike IT-MS which operates tandem MS fragmentation solely in time, QTOF-MS and other hybrid MS instruments operate tandem MS fragmentation in time and space. [23] Moreover, QTOF-MS methods give a holistic view of the molecule's fragmentation patterns as opposed to IT-MS which excludes other ions and focuses on pre-selected ions in MS^n methods. In the current study, various QTOF-MS settings (capillary and cone voltage) were optimized to induce any underlying fragmentation patterns between UV-generated geometrical isomers of 3,5-diCQA.

EXPERIMENTAL

Chemicals

Authentic standards of *trans* mono-caffeoylquinic acids (3-, 4-, and 5-CQA) and dicaffeoylquinic acids (1,3-diCQA, 1,5-diCQA, 3,4-diCQA, 3,5-diCQA and 4,5-diCQA) were purchased from Phytolab (Vestenbergsgreuth, Germany). Analytical grade methanol and acetonitrile were obtained from Romil (Cambridge, UK). Deionised milli-Q water was generated using a Milli-Q Gradient A10 system (Millipore, MA, USA). All other chemicals, such as formic acid (FA) and leucine enkaphalin were purchased from Sigma-Aldrich (St. Louis, MO, USA).

Sample preparation

To obtain the *cis* isomers of the caffeoylquinic and dicaffeoylquinic acids a 1 mg/mL stock solution was prepared in 100% methanol. The samples were then irradiated for 5 h at 245 nm using a UV box (Spectroline, USA).

UHPLC-ESI -QTOF-MS analyses

During chromatographic separation, 3.0 µL of the sample was injected and separated using an HSS T3 C_{18} reversed-phase column (150 mm x 2.1 mm, 1.8 µm; Waters Corporation, MA, USA). The mobile phase consisted of milli-Q water containing 0.1% FA (Eluent A) and acetonitrile containing 0.1% FA (Eluent B). The gradient elution and separation was achieved at a constant flow rate of 0.6 ml/min as follows: 15% B was kept constant for14 min followed by a rapid gradient of 15-100% B over 1 min, and kept at 100% B for 2 min and

another gradient of 100 -15% B over 1 min and a final equilibration step with 15 % B was carried out for 2 min. For the alkali metal studies, a 10 mM aqueous solution of alkali metal chloride salts was infused into the main eluent stream through the on-board syringe drive at a constant flow rate of 2 µL/min before entering the MS ion source. For MS detection a SYNAPT G1 Q-TOF-MS (Waters Corporation MA, USA) was used. The MS was operated in V-optics mode and all the analyses were carried out in ESI negative ionisation mode utilising the following conditions: extraction cone voltage at 4 V, source temperature at 120 $^{\circ}$C, desolvation temperature at 450 $^{\circ}$C, cone gas flow rate of 50 L/h, desolvation gas flow rate of 550 L/h. The mass range for detection was from *m/z* 50 to 1000 with a scan time of 0.1 s and an interscan time of 0.02 s. For ISCID, sampling cone voltages of 10, 25, 40 and 60 V were used and the capillary voltages were 1.0, 1.5, 2.0, 2.5, 3.0 and 3.5 kV. Further fragmentation of these isomers was achieved by ramping the collision energy levels from 3 to 40 eV.

Statistical analysis

For statistical analyses of the initial optimization of ESI-MS conditions needed for efficient discrimination between the geometrical isomers of 3,5-diCQA, Statistica 12 software (Dell, USA) was used. Here, responsive surface models (RSM) and *Pareto* charts were computed and used to show the statistical significance of the tested MS parameters namely cone and capillary voltages.

RESULTS AND DISCUSSION

Currently, the tentative identification of geometrical isomers of CGAs is achieved through the use of chromatographic retention profiles on reverse phase (RP) columns. [8] Though a useful method for CGA characterisation, inconsistencies in the elution order of the geometrical isomers have resulted from the lack of standardised chromatography and experimental conditions. Work done elsewhere, where CQA samples were irradiated at 366 nm [24] instead of the short wavelength of 245 nm normally used, showed differences in the chromatographic elution profile from what has been previously reported. [8,20] As such, an ISCID UHPLC/QTOF-MS method was optimized to discriminate between the geometrical isomers of diCQA. ISCID allows for CID to occur in the ion source of mass spectrometer to give similar fragmentation patterns to those obtained with MS/MS methods without the need of pre-selection of desired ions. [25,26] Initial chromatographic conditions were optimized to result in efficient separation of the four geometrical isomers of 3,5-diCQA (Scheme 1, Fig.

1). It should be mentioned that other diCQA regioisomers (1,3-diCQA, 1,5-diCQA, 3,4-diCQA, and 4,5-diCQA) were also studied and they were all shown to result in a similar trend. For consistency, most of the results presented within this manuscript were achieved with 3,5-diCQA isomers. The results of the other regioisomers are also discussed throughout the manuscript with most of the results in the supplementary files.

UV-irradiated samples of 3,5-diCQA were subjected to varying conditions of cone voltage and capillary voltage in order to induce differential MS fragmentation patterns. Only the optimized conditions, i.e. MS conditions that best showed the differences in alkali metal adduct formation between the geometrical isomers, were used for the analyses of other regioisomers of diCQA. To distinguish between the *cis* and *trans* isomers, peaks that increased in abundance/intensity as a result of UV-irradiation compared to the non-irradiated control sample (which contains only the all *trans* isomer), were assigned as *cis* isomer peaks (Fig. 1; S1-S4). To distinguish between the generated *cis* isomers of 3,5-diCQA, peak I (Fig. 1) which was produced in minor concentration was designated as the *cis*-*cis* (di-*cis*) isomer since it has also been reported to be produced in trace amounts. [8, 10] Furthermore, the other two peaks, III and IV (Fig. 1) were designated as mono-*cis* 1 (3^{cis}, 5^{trans}-diCQA) and mono *cis* 2 (3^{trans}, 5^{cis} -diCQA). The two *mono-cis* isomers, however, could not be precisely differentiated as they were produced in relatively equal abundance, contrary to the 1:4 ratio that was reported elsewhere. [10] However, an inference can be made based on the available information on the hydrophobicities of the mono-acyl CGAs. It has previously been shown that the *cis* isomers formed due to UV radiation, change the hydrophobicity of the mono-acylated CGAs significantly.[8] For instance, an increase in hydrophobicity of *cis*-5-monoacyl CGAs has been noted and, as such, the *cis* geometrical isomers of 5-monoacyl CGAs elute later than their *trans* counterparts in reverse phase chromatography. [8, 27] However, an opposite case is observed for 3- and 4-monoacyl CGAs where the *cis* isomers elute earlier than their *trans* counterparts. [8,27] The increase or decrease in hydrophobicity of these molecules has been linked to their ability or inability to form intramolecular hydrogen bonds (IHB) [8] Therefore, if an assumption is made that the hydrophobicity effects seen in the mono-acyl CGAs are additive, then we would expect the mono-*cis* isomer with the greater retention time to have the *cis* configuration on the caffeoyl moiety acylated on the 5' position of the quinic acid, thus the 3^{trans}, 5^{cis}-diCQA. Interestingly, our preliminary quantum theoretical calculations using the B3LYP/6-31G(d, p) method (both in methanol and *in vacuo*) indicated the 3^{trans}, 5^{cis}-diCQA mono *cis* isomer to be slightly more energetically favourable than the 3^{cis}, 5^{trans}-diCQA mono *cis* isomer, due to stronger intramolecular

hydrogen bonds found in the former isomer. Furthermore, the 3^{trans}, 5^{cis}-diCQA mono *cis* isomer was also found to have a smaller dipole moment than all the geometrical isomers of 3,5-diCQA, suggesting that it is more hydrophobic, which could be the reason for its late elution compared to the other geometrical isomers (Peak IV, Fig. 1). By extension, the same phenomenon can also be supported by the elution profiles of other diCQA molecules with acylation on the 5' position of the quinic acid such as 1,5-diCQA and 4,5-diCQA. One of the mono *cis* isomers of these diCQA molecules (1,5-diCQA and 4,5-diCQA) elutes later than their *trans* counterpart (Fig. S2 and Fig. S4), suggesting that the same phenomenon of *cis* isomerism at the 5' position of quinic acid may also play a role in increasing the hydrophobicity of these mono-*cis* diCQAs.

During IT-MS, 3,5-diCQA (with $[M-H]^-$ of *m/z* 515) consistently produces diagnostic markers at *m/z* 353 $[M-H-162]^-$ due to the loss of one caffeoyl moiety which produces a base peak ion at MS^2 level. At MS^3, a base peak at *m/z* 191[quinic acid-H]$^-$ and a secondary peak at *m/z* 179 [caffeic acid-H]$^-$ with a consistent ratio of approximately 2:1 are produced. [8, 20] Similarly, in the current study, the same ions were observed for all four geometrical isomers using our optimized QTOF-MS method (Fig. 2; Fig. 3; Fig. S5). Optimisation of the in-source QTOF-MS conditions by changing the capillary and cone voltages was carried out, and interestingly, there were minimal fragmentation differences between the isomers due to changes in the capillary voltage but significant differences were noted due to changes in the cone voltage (Fig. S6 and Fig. S7). From the results, it was observed that at a capillary voltage of 3.5 kV and cone voltage of 60 V, the three *cis* isomers (Fig. 1; peaks I, III and IV), had an intense peak at *m/z* 375.065 $[M-2H-162 + Na]^-$ as compared to the trans isomer which showed an intense peak at *m/z* 353.082 $[M-H-162]^-$ due to the loss of one caffeic acid moiety (Fig. 2). For the *trans* isomer the peak at *m/z* 353.082 $[M-H-162]^-$ was much more intense than that of the sodium adduct at *m/z* 375.065. [28] Between the *cis* isomers, the *cis-cis* isomer was observed to form more of the sodium adduct (*m/z* 375.065) relative to the deprotonated caffeoylquinic acid fragment (*m/z* 353.082) than the other two mono-*cis* isomers (Fig. 2). Comparing the two *mono-cis* isomers it was found that one of them, 3^{trans}, 5^{cis}-diCQA, (Fig. 2B) displayed a higher tendency to form the sodium adduct than 3^{cis}, 5^{trans}, (Fig. 2C), even though the difference is very minimal.

Our preliminary tandem MS (MS^2) results on the deprotonated sodium adduct $[M-2H+Na]^-$ did not show any differences between the isomers. As mentioned above, the differences between the geometrical isomers were more pronounced at elevated cone and capillary voltages (Fig. S6), however, changes in cone voltages were found to have a more

significant effect than changes in capillary voltage (Fig. S7). This could be attributed to the fact that changes in the MS, cone voltage causes an increase in the internal energy of the molecular ions which induces greater fragmentation while the capillary voltage is concerned with the production of the ion plume in front of the sample cone. [27,28] By selecting/trapping a specific ion for further fragmentation, the nuances are lost and fragmentation patterns are the same, whereas when all ions are allowed to reach the detector a more holistic view is achieved. Analyses in space allow 'real-time' analysis since a continuous beam of ions reaches the detector without filtering others (such as metal adduct in this case). [23,29,30] As such, our ISCID method can therefore be regarded as superior in showing the underlying differences between the geometrical isomers of diCQA, a phenomenon that has been deemed impossible hitherto.

To further confirm these metal-binding preferences by the *cis* isomers, and to eliminate any possibility that our observations are limited to one regioisomer (3,5-diCQA in this case), we also investigated other diCQA regioisomers (1,3-diCQA, 1,5-diCQA, 3,4-diCQA, and 4,5-diCQA) (Fig. S8 - S11). Furthermore, mobile phases spiked with other alkali metals ions (lithium and potassium), were also investigated for all the diCQA regioisomers. When the chromatographic mobile phase was spiked with lithium (Li^+), similar results to those observed with Na^+ were achieved; here the *cis-cis* isomer of 3,5-diCQA (Fig. 3) and of 4,5-diCQA (Fig. 4) which were found to bind preferentially to the Li^+ ion compared to the *trans-trans* isomer as seen with the peak at *m/z* 359.091 $[M-2H-162+Li]^-$. The other two *mono-cis* isomers also showed preference for the Li^+, with the 3^{trans}, 5^{cis} mono-*cis* isomer (peak IV, Fig. 1; Fig. 3) showing slightly greater affinity than the 3^{cis}, 5^{trans} mono-*cis* isomer (peak III, Fig. 1; Fig. 3). The same phenomenon was also observed with other positional isomers (Figs. S12 - S14). The preferential metal adduct formation by the *cis* geometrical isomers of the various regioisomers can also be seen with the peaks of un-fragmented adduct ions ($[M-2H+Metal\ ion]^-$) (Fig. 2 - 5; Fig. S5, S8 - S17). Closer visual inspection of the mass spectra of the geometrical isomers also shows another noteworthy trend where detection of two independent MS occurrences seems to exist in one spectrum. Here, the deprotonated molecule ions at *m/z* 515$[M-H]^-$ fragment to give a product ion at *m/z* 353 $[M-H-162]^-$. Whilst on the other hand the adduct ions $[M-2H + Na]^-$ at *m/z* 537, $[M-2H + Li]^-$ at *m/z* 521 and $[M-2H + K]^-$ at *m/z* 553 give rise to product ions at *m/z* 375, 359 and 391, respectively. As seen throughout the manuscript thus far, the peak intensity ratio of the adducted precursor ion after losing one caffeoyl moiety ($[M-2H-162 +Metal\ ion]^-$) over the intensity of non-adducted precursor ion after losing one caffeoyl moiety ($[M-H-162]^-$) was used to assign metal

preference for the *cis* isomers over their *trans* isomer counterparts. Our results further show other higher order adduct ions which also clearly show the adduct formation preference of the *cis* isomers over their *trans* counterparts. Here for instance, when considering 4,5-diCQA, its *cis* isomers can be discriminated from their *trans* counterpart by looking at the intensities of the double deprotonated and triple deprotonated metal adducts ions containing one or two metal ions, respectively (Fig. 4). Furthermore, the existence of these higher order adducts such as $[M-4H+ 3Li]^-$ at *m/z* 533.142 and $[M-3H+ 2K]^-$ at *m/z* 591.027 (Fig. 4 and Fig. 5) can be exploited in future using more directed MS/MS or MS^n for alternative methods which can be used for definite identification of geometrical isomers of these phenolics and other related compounds.

Studies done on the mono-acyl CQAs showed a similar but less pronounced trend as seen for the diCQAs (Fig. S18 - S20) suggesting possible differences in the chelation ability or coordination mechanism between the two structural hierarchies of the CQAs, with the diCQA being superior. Here, our results show that the *cis* isomers of the mono-acyl CQAs formed the sodium adduct (*m/z* 375.066) more than their *trans* counterparts. Moreover, amongst the mono-acyl CQAs, the 5-CQA regioisomer had a greater tendency to form the sodium adduct than the 3- and 4-CQA regioisomers. This further highlights the differences in alkali metal binding preferences to be more pronounced on the cis-geometrical isomers of CQAs regardless of the structural hierarchy (mono and di-acylated CQA in this case). However, as previously stated, to achieve these underlying differences, MS optimization should be carried out by either varying cone voltage or capillary voltage as indicated herein.

The use of metal additives has previously been shown to be a valuable tool for MS based studies of isomeric and isobaric compounds. [31, 32, 33] Zhang and Brodbelt, [31] using silver ions as an additive, were able to not only distinguish between various isomers of flavonoid glycosides, but were able to obtain structural information such as the site of glycosylation on the flavonoid. The metal binding of catechol-containing molecules has also been known for a long time with serious biological and chemical implications.[34] In mass spectrometry studies, the metal binding/chelation by catechol-containing flavonoids has been noted and used to discriminate between closely related molecules.[35] In the current study, the molecules under investigation also possess catechol units (Scheme 1) and this is believed to play a role in the chelation of the alkali metals. In the past, depending on the metals used, different stoichiometric ratios between the ligands and alkali metals have also been noted elsewhere. [36] From a close visual inspection of the different geometrical isomers of diCQA it can be seen that the catechol unit of these isomers is very similar and, as such, the differences

in metal preference are not obvious. However, our preliminary quantum theoretical calculations using the B3LYP/6-31G(d,p) method have indicated more stable adducts formed by *cis* isomers of 3,5-diCQA owing to multiple coordinating groups around the alkali metal due to a bent configuration which is absent in the *trans* configuration (results not shown). Therefore, the *cis* isomers are expected to retain the metals even at elevated cone and collision energies before and after fragmentation.

From our findings, it is evident that the consistent alkali metal adduct preference by *cis* geometrical isomers of the diCQA regioisomers, in conjunction with ISCID-QTOF/MS, may be used as a means of differentiating these molecules from one another, a phenomenon which has been deemed impossible with multi-stage IT-MS based approaches. [8,10] The current results can be expanded by investigating other metal adducts of higher orders as they are expected to result in ions of different intensities which can further be exploited for the discrimination of these geometrical isomers. The use of other forms of additives or chemical modifications other than metals, has recently been applied for proper annotation of diCQAs elsewhere. [36] Our results are expected to further buttress the already established method of discriminating between these isomers which, to date, is based only on the chromatographic elution profile. [8] This MS-based method allows for the annotation of these complex molecules in the case where different chromatographic conditions are applied.

From our results, it is evident that more research in the field of phytochemical analysis is needed, especially for the characterization of plant metabolites with health benefits. The biological activity of such metabolites depends not only on their functional groups, but also on the spatial structural arrangement of these groups. [37] Thus, isomerisation of biologically active metabolites may affect their potency. For example, Chen et al. [38] found that the photo-isomerization of *trans*-cinnamic acid to *cis*-cinnamic acid affected its anti-mycobacterial activity. Therefore, the accurate distinction of such isomers using analytical techniques such as MS is very important for quality control purposes.

CONCLUSION

An ISCID-QTOF/MS based method has been developed for the discrimination of geometrical isomers of diCQAs. The results of our study have demonstrated, for the first time, recognisable differences in fragmentation patterns of geometrical isomers of CGA molecules. Here, *cis* geometrical isomers of the diCQAs were shown to have greater affinity for alkali metals (Na, Li and K cations) compared to their *trans* counterparts during MS analyses in negative ionisation mode. The observation of this same trend in the mono-acyl CQAs shows

that this preferential alkali metal binding of the *cis* isomers is not limited by structural hierarchy or to specific regioisomers. This also suggests that other molecules in the CGA class of compounds may exhibit the same trend. Under well optimized conditions, an interesting trend between the *cis* isomers was noted, where some molecules had greater affinity for the alkali metal ions in comparison to the other *cis* isomers. Our results, therefore, encourage the use of different MS technologies to achieve a holistic view of the mechanistic fragmentation chemistry which can further be exploited for efficient and precise metabolite identification purposes. To achieve the above, other adduct ions of higher orders can be studied using more directed tandem MS methods (MS/MS or MS^n) in combination with quantum theoretical calculations. Thus our results encourage the advancement of the well-known hierarchical key methods of CGA annotations to include the annotation of geometrical isomers thereof, based on alkali metal adduct preferences. [39, 40, 41, 42]

ACKNOWLEDGEMENTS

The University of Johannesburg and the South African National Research Foundation (NRF) are thanked for fellowship support (MM) and financial support (NEM, grant number TTK1306111889).

SUPPLEMENTARY FIGURES AND TABLES

Figure S1: A representative UHPLC-Q-TOF-MS base peak intensity (BPI) chromatogram showing the separation of different geometrical isomers of 1,3-diCQA generated during UV exposure. Peak I: di-*trans*, peak II: mono-*cis* 1and peak III: mono-*cis* 2.

Figure S2: A representative UHPLC-Q-TOF-MS base peak intensity (BPI) chromatogram showing the separation of different geometrical isomers of 1,5-diCQA generated during UV exposure. Peak I: di-*trans*, peak II: mono-*cis* 1 and peak III: mono-*cis* 2.

Figure S3: A representative UHPLC-Q-TOF-MS base peak intensity (BPI) chromatogram showing the separation of different geometrical isomers of 3,4-diCQA generated during UV exposure. Peak I: di-*cis* isomer, peak II: di-*trans*, peak III: mono-*cis* 1 and peak IV: mono-*cis* 2.

Figure S4: A representative UHPLC-Q-TOF-MS base peak intensity (BPI) chromatogram showing the separation of different geometrical isomers of 4,5-diCQA generated during UV exposure. Peak I: mono-*cis* 1, peak II: di-*trans*, peak III: di-*cis* isomer and peak IV: mono-*cis* 2.

Figure S5: Representative Q-TOF-MS spectra for the (A) di-*trans*, (B) mono-*cis* 1, (C) mono-*cis* 2, and (D) *di-cis* geometrical isomers of 3,5-diCQA with the differentiating diagnostic potassium adduct $[M-3H+2K]^-$ seen at *m/z* 591.027.

Figure S6: Responsive surface model for the optimum MS conditions for efficient discrimination of the geometrical isomers of 3,5-diCQA. A) di-*trans* and B) di-*cis* 3,5-diCQA

Figure S7: Standardized *Pareto* charts for the effects of capillary and cone voltage on the *m/z* 375/353 peak ratio.

Figure S8: Representative Q-TOF-MS spectra for the (A) di-*trans,* (B) mono-*cis* 1 and (C) mono-*cis* 2 of 1,3-diCQA with the differentiating diagnostic sodium adduct $[M-3H-179+Na]^-$ peak seen at *m/z* 357.057.

Figure S9: Representative Q-TOF-MS spectra for the (A) di-*trans* , (B) mono-*cis* 1 and (C) mono-*cis* 2 geometrical isomers of 1,5-diCQA with the differentiating diagnostic sodium adduct $[M-3H-179+Na]^-$ peak seen at *m/z* 357.056.

Figure S10: Representative Q-TOF-MS spectra for the (A) di-*trans*, (B) mono-*cis* 1, (C) mono-*cis* 2, and (D) *di-cis* geometrical isomers of 3,4-diCQA with the differentiating diagnostic sodium adduct $[M-2H+Na]^-$ peak seen at *m/z* 537.099.

Figure S11: Representative Q-TOF-MS spectra for the (A) di-*trans*, (B) mono-*cis* 1, (C) mono-*cis* 2, and (D) *di-cis* geometrical isomers of 4,5-diCQA with the differentiating diagnostic sodium adduct $[M-2H+Na]^-$ peak seen at *m/z* 537.097.

Figure S12: Representative Q-TOF-MS spectra for the (A) di-*trans*, (B) mono-*cis* 1 and (C) mono-*cis* 2 geometrical isomers of 1,3-diCQA with the differentiating diagnostic lithium adduct $[M-3H-179+Li]^-$ peak seen at *m/z* 341.081.

Figure S13: Representative Q-TOF-MS spectra for the (A) di-*trans*, (B) mono-*cis* 1 and (C) mono-*cis* 2 geometrical isomers of 1,5-diCQA with the differentiating diagnostic Lithium adduct $[M-3H-179+Li]^-$ peak seen at *m/z* 341.082.

Figure S14: Representative Q-TOF-MS spectra for the (A) di-*trans*, (B) mono-*cis* 1, (C) mono-*cis* 2, and (D) *di-cis* geometrical isomers of 3,4-diCQA with the differentiating diagnostic lithium adduct $[M-2H+Li]^-$ peak seen at *m/z* 521.126.

Figure S15: Representative Q-TOF-MS spectra for the (A) di-*trans* and (B) mono-*cis* 1/2 geometrical isomers of 1,3-diCQA with the differentiating diagnostic potassium adduct $[M-3H+2K]^-$ seen at *m/z* 591.030

Figure S16: Representative Q-TOF-MS spectra for the (A) di-*trans*, (B) mono-*cis* 1 and (C) mono-*cis* 2 geometrical isomers of 1,5-diCQA with the differentiating diagnostic potassium adduct $[M-3H+2K]^-$ seen at *m/z* 591.024.

Figure S 17: Representative Q-TOF-MS spectra for the (A) di-*trans*, (B) mono-*cis* 1, (C) mono-*cis* 2, and (D) *di-cis* geometrical isomers of 4,5-diCQA with the differentiating diagnostic potassium adduct [M-3H+2K] seen at *m/z* 591.031.

Figure S18: Ion spectra for the (A) *trans* and (B) *cis* isomers of 5 CQA. 375/353 peak ratio: *trans* (1.85), *cis* (2.48).

Figure S19: Ion spectra for the (A) *trans* and (B) *cis* isomers of 4 CQA. 375/353 peak ratio: *trans* (0.44), *cis* (0.58).

Figure S20: Ion spectra for the (A) *trans* and (B) *cis* isomers of 3 CQA. 375/353 peak ratio: *trans* (0.67), *cis* (0.48).

Table S1: Diagnostic fragment peaks for 1,3 diCQA for the different alkali metals.

Table S2: Diagnostic fragment peaks for 1,5 diCQA for the different alkali metals

Table S3: Diagnostic fragment peaks for 3,4 diCQA for the different alkali metals

Table S4: Diagnostic fragment peaks for 3,5 diCQA for the different alkali metals

Table S5: Diagnostic fragment peaks for 4,5 diCQA for the different alkali metals

SCHEME AND FIGURE LEGENDS

Scheme 1. Structures of the dicaffeoylquinic acid regioisomers.

Figure 1. A representative UHPLC-Q-TOF-MS base peak intensity (BPI) chromatogram showing the separation of different geometrical isomers of 3,5-diCQA generated during UV exposure. Peak I: di-*cis* isomer, peak II: di-*trans*, peak III: mono-*cis* 1 and peak IV: mono-*cis* 2.

Figure 2. Representative Q-TOF-MS spectra for the (A) di-*trans*, (B) mono-*cis* 1, (C) mono-*cis* 2, and (D) *di-cis* geometrical isomers of 3,5-diCQA with the differentiating diagnostic sodium adduct $[M-2H-162+Na]^-$ peak seen at *m/z* 375.065.

Figure 3. Representative Q-TOF-MS spectra for the (A) di-*trans*, (B) mono-*cis* 1, (C) mono-*cis* 2, and (D) di-*cis* geometrical isomers of 3,5-diCQA with the differentiating diagnostic lithium adduct $[M-2H-162+Li]^-$ peak seen at *m/z* 359.091.

Figure 4. Representative Q-TOF-MS spectra for the (A) di-*trans*, (B) mono-*cis* 1, (C) mono-*cis* 2, and (D) *di-cis* geometrical isomers of 4,5-diCQA with the differentiating diagnostic lithium adduct $[M-2H-162+Li]^-$ peak seen at *m/z* 359.0893.

Figure 5. Representative Q-TOF-MS spectra for the (A) di-*trans*, (B) mono-*cis* 1, (C) mono-*cis* 2, and (D) *di-cis* geometrical isomers of 3,4-diCQA with the differentiating diagnostic potassium adduct $[M-3H+2K]^-$ peak seen at *m/z* 591.0276.

REFERENCES

[1] M.N. Clifford. Chlorogenic acids and other cinnamates- nature, occurrence and dietary burden. *J. Sci. Food Agr.* **1999**, 79, 362.

[2] M.N. Clifford. Chlorogenic acids and other cinnamates - nature, occurrence, dietary burden, absorption and metabolism. *J. Sci. Food Agr.* **2000**, 80, 1033.

[3] R. Jaiswal, T. Sovdat, F. Vivan, N. Kuhnert. Profiling and characterization by LC-MS^n of the chlorogenic acids and hydroxycinnamoylshikimate esters in Maté (*Ilex paraguariensis*). *J. Agr. Food Chem.* **2010**, *58*, 5471.

[4] K. Schütz, D. Kammerer, R. Carle, A. Schieber. Identification of caffeoylquinic acids and flavonoids from artichoke (*Cynara scolymus* L.) heads, juice, and pomace by HPLC-DAD-ESI/MS^n. *J. Agr. Food Chem.* **2004**, 52, 4090.

[5] A. Könczöl, Z. Béni, M.M. Sipos, A. Rill, V. Háda, J. Hohmann, I. Mathec, C. Szantay, G.M. Keseru, G.T. Balogh. Antioxidant activity-guided phytochemical investigation of *Artemisia gmelinii* Webb. Ex Stechm.: Isolation and spectroscopic challenges of 3,5-O-dicaffeoyl (epi?) quinic acid and its ethyl ester. *J. Pharm. Biomed. Anal*. **2012**, 59, 83.

[6] H. Tamura, T. Akioka, K. Ueno, T. Chujyo, K. Okazaki, P.J. King, W.E. Robinson Jr. Anti-human immunodeficiency virus activity of 3,4,5-tricaffeoylquinic acid in cultured cells of lettuce leaves. *Mol. Nutr. Food Res.* **2006**, 50, 396.

[7] S. Hong, T. Joo, J.W. Jhoo. Antioxidant and anti-inflammatory activities of 3,5-dicaffeoylquinic acid isolated from *Ligularia fischeri* leaves. *Food Sci. Biotech.* **2015**, 24, 257.

[8] M.N. Clifford, J. Kirkpatrick, N. Kuhnert, H. Roozendaal, P.R. Salgado. LC-MS^n of the *cis* isomers of chlorogenic acids. *Food Chem.* **2008**, 106, 379.

[9] L. Li, Z. Wang, Y. Peng, X. Fu, Y. Wang, W. Xiao, S. Song. Screening and identification of multi-components in *Re Du Ning* injections using LC/TOF-MS with UV-irradiation. *J. Chromtogr. Sci.* **2015**, 53, 778.

[10] H. Karaköse, R. Jaiswal, S. Deshpande, N. Kuhnert. Investigation of the photochemical changes of chlorogenic acids induced by ultraviolet light in model systems and in agricultural practice with *Stevia rebaudiana* cultivation as an example. *J. Agr. Food Chem.* **2015**, 63, 3338.

[11] Z. Fu, Z. Li, P. Hu, Q. Feng, R. Xue, Y. Hu, C. Huang. A practical method for the rapid detection and structural characterization of major constituents from traditional Chinese medical formulas: analysis of multiple constituents in Yinchenhao Decoction. *Anal. Meth.* **2015**, 7, 4678.

[12] J. Mouton, F. Van der Kooy. Identification of *cis*- and *trans*- melilotoside within an *Artemisia annua* tea infusion. *Eur. J. Med. Plants* **2014**, 4, 52.

[13] E. N. Ncube, M.I. Mhlongo, L.A. Piater, P.A. Steenkamp, I.A. Dubery, N.E. Madala. Analyses of chlorogenic acids and related cinnamic acid derivatives from *Nicotiana tabacum* tissues with the aid of UPLC-QTOF-MS/MS based on the in-source collision-induced dissociation method. *Chem. Cent. J.* **2014**, 8, 1.

[14] N.E. Madala, P.A. Steenkamp, L.A. Piater, I.A. Dubery. Collision energy alteration during mass spectrometric acquisition is essential to ensure unbiased metabolomics analysis. *Anal. Bioanal. Chem.* **2012**, 404, 367.

[15] A. Aharoni, R.C. de Vos, H.A. Verhoeven, C.A. Maliepaard, G. Kruppa, R.J. Bino, D.B. Goodenowe. Nontargeted metabolome analysis by use of Fourier transform ion cyclotron mass spectrometry. *OMICS*. **2002**, 6, 217.

[16] O. Fiehn, J. Kopka, R.N. Trethewey, L. Willmitzer. Identification of uncommon plant metabolites based on calculation of elemental compositions using gas chromatography and quadrupole mass spectrometry. *Anal. Chem.* **2000**, 72, 3573.

[17] R.C. de Vos, S. Moco, A. Lommen, J.J. Keurentjes, R.J. Bino, R.D. Hall. (2007). Untargeted large-scale plant metabolomics using liquid chromatography coupled to mass spectrometry. *Nature Protocols*. **2007**, 2, 778.

[18] M.N. Clifford, W. Wu, J. Kirkpatrick, R. Jaiswal, N. Kuhnert. Profiling and characterisation by liquid chromatography/multi-stage mass spectrometry of the chlorogenic acids in *Gardeniae Fructus*. *Rapid Commun. Mass Spectrom.* **2010**, 24, 3109.

[19] R. Jaiswal, M.A. Patras, P.J. Eravuchira, N. Kuhnert. Profile and characterization of the chlorogenic acids in green Robusta coffee beans by LC-MS^n: Identification of seven new classes of compounds. *J. Agr. Food Chem.* **2010**, 58, 8722.

[20] M.N. Clifford, K.L. Johnston, S. Knight, N. Kuhnert. Discriminating between the six isomers of dicaffeoylquinic acid by LC-MS^n. *J. Agric. Food Chem.* **2005**, 53, 3821.

[21] Y. Jiang, B. David, P. Tu, Y. Barbin. Recent analytical approaches in quality control of traditional Chinese medicines. *Anal. Chim. Acta.* **2010**, 657, 9.

[22] N.E. Madala, F. Tugizimana, P.A. Steenkamp. (2014). Development and optimization of an UPLC-QTOF-MS/MS method based on an in-source collision induced dissociation approach for comprehensive discrimination of chlorogenic acids isomers from *Momordica* plant species. *J. Anal. Methods Chem.* **2014**, 650879.

[23] R.M. Alonso-Salces, C. Guilloi, L.A. Berrueta. Liquid chromatography coupled with ultraviolet absorbance detection, electrospray ionization, collision induced dissociation and tandem mass spectrometry on a triple quadrupole for the on-line characterization of polyphenols and methylxanthines in green coffee beans. *Rapid Commun. Mass Spectrom.* **2009**, 23, 363.

[24] L. Barros, M. Dueñas, A.M. Carvalho, I.C.F.R. Ferreira, C. Santos-Buelga. Characterization of phenolic compounds in flowers of wild medicinal plants from Northeastern Portugal. *Food Chem. Toxicol.* **2012**, 50, 1576.

[25] L. Hua, K. Hou, P. Chen, Y. Xie, J. Jiang, Y. Wang, W. Wang, H. Li. Realization of in-source collision-induced dissociation in single-photon ionization time-of-flight mass spectrometry and its application for differentiation of isobaric compounds. *Anal. Chem.* **2015**, 87, 2427.

[26] E. Schramm, A. Kürten, J. Hölzer, S. Mitschke, F. Mühlberger, M. Sklorz, J. Wieser, A. Ulrich, M. Pütz, R. Schulte-Ladbeck, R. Schultze, J. Curtius, S. Borrmann, R. Zimmermann. Trace detection of organic compounds in complex sample matrixes by single photon ionization ion trap mass spectrometry: real-time detection of security-relevant compounds and online analysis of the coffee-roasting process. *Anal. Chem.* **2009**, 81, 4456.

[27] C. Xie, K. Yu, D. Zhong, T. Yuan, F. Ye, J.A. Jarrell, A. Miller, X. Chen. Investigation of isomeric transformations of chlorogenic acid in buffers and biological matrixes by ultraperformance liquid chromatography coupled with hybrid quadrupole/ ion mobility/ orthogonal acceleration time-of-flight mass spectrometry. *J. Agric. Food Chem.* **2011,** 59, 11078.

[28] A.G. Harrison. Energy resolved mass spectrometry: a comparison of quadrupole cell and cone-voltage collision-induced dissociation. *Rapid Commun. Mass Spectrom.* **1999**, 13, 1663.

[29] A. Tolonen, T. Joutsamo, S. Mattlla, T. Kämäräinen, J. Jalonen. Identification of isomeric dicaffeoylquinic acids from *Eleutherococcus senticosus* using HPLC-ESI/TOF/MS and ^{1}H-NMR methods. *Phytochem. Anal.* **2002**, 13, 316.

[30] A.G. Frenich, P. Plaza-Bolaños, J.L. Martínez Vidal. Comparison of tandem-in-space and tandem-in-time mass spectrometry in gas chromatography determination of pesticides: Application to simple and complex food samples. *J. Chrom.* **2008**, 1203, 229.

[31] J. Zhang, J.S. Brodbelt. Silver complexation and tandem mass spectrometry for differentiation of isomeric flavonoid diglycosides. *Anal. Chem.* **2005**, 77, 1761.

[32] A.M. Cirigliano, G.M. Cabrera. Differentiation of cyclosporin A from isocyclosporin A by liquid chromatography/electrospray ionization mass spectrometry with post-column addition of divalent metal salt. *Rapid Commun. Mass Spectrom.* **2014**, 28, 465.

[33] H.T. Pham, A. J. Trevitt, T. W. Mitchell, S. J. Blanksby. Rapid differentiation of isomeric lipids by photodissociation mass spectrometry of fatty acid derivatives. *Rapid Commun. Mass Spectrom.* **2013**, 27, 805.

[34] N. Schweigert, A.J. Zehnder, R.I. Eggen. Chemical properties of catechols and their molecular modes of toxic action in cells, from microorganisms to mammals. *Environ. Microbiol.* **2001**, 3, 81.

[35] M.T. Fernandez, M.L. Mira, M.H. Florencio, K.R. Jennings. (2002). Iron and copper chelation by flavonoids: an electrospray mass spectrometry study. *J. Inorg. Biochem.* **2002,** 92, 105.

[36] D. Cunningham, P. McArdle, M. Mitchell, N. Ní Chonchubhair, M. O'Gara, F. Franceschi, C. Floriani, C. Adduct formation between alkali metal ions and divalent metal salicylaldimine complexes having methoxy substituents. A structural investigation. *Inorg. Chem.* **2000,** 39, 1639.

[37] J. McConathy, M.J. Owens. Stereochemistry in drug action. *J. Clin. Psychiatry* **2003**, 5, 70.

[38] Y.L. Chen, S.T. Huang, F.M. Sun, Y.L. Chiang, C.J. Chiang, C.M. Tsai, C.J. Weng. (2011). Transformation of cinnamic acid from *trans*- to *cis*-form raises a notable bactericidal and synergistic activity against multiple-drug resistant *Mycobacterium tuberculosis*. *Eur. J. Pharm. Sci.* **2011**, 43, 188.

[39] M.N. Clifford, S. Knight, N. Kuhnert. Discriminating between the six isomers of dicaffeoylquinic acid by LC-MS^n. *J. Agri. Food Chem.* **2005,** 53, 3821.

[40] M.N. Clifford, K.L. Johnston, S. Knight, N. Kuhnert. Hierarchical scheme for LC-MS^n identification of chlorogenic acids. *J. Agri. Food Chem.* **2003**, 51, 2900.

[41] L. Bravo, L. Goya, E. Lecumberri. LC/MS characterization of phenolic constituents of mate (*Ilex paraguariensis*, St. Hil.) and its antioxidant activity compared to commonly consumed beverages. *Food Res. Int.* **2007,** 40, 393.

[42] N. Dartora, L.M. De Souza, A.P. Santana-Filho, M. Iacomini, A.T. Valduga, P. A. Gorin, G.L. Sassaki. UPLC-PDA–MS evaluation of bioactive compounds from leaves of *Ilex paraguariensis* with different growth conditions, treatments and ageing. *Food Chem.* **2011**, 129, 1453.

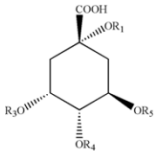

Q

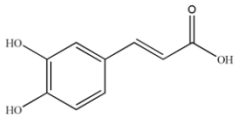

trans-C

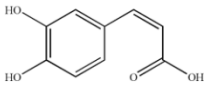

cis-C

Name	**R_1**	**R_3**	**R_4**	**R_5**
1-*trans*, 3-*trans*-dicaffeoylquinic acid	*trans*-C	*trans*-C	H	H
1-*trans*, 3-*cis*-dicaffeoylquinic acid	*trans*-C	*cis*-C	H	H
1-*cis*, 3-*trans*-dicaffeoylquinic acid	*cis*-C	*trans*-C	H	H
1-*cis*, 3-*cis*-dicaffeoylquinic acid	*cis*-C	*cis*-C	H	H
1-*trans*, 5-*trans*-dicaffeoylquinic acid	*trans*-C	H	H	*trans*-C
1-*trans*, 5-*cis*-dicaffeoylquinic acid	*trans*-C	H	H	*cis*-C
1-*cis*, 5-*trans*-dicaffeoylquinic acid	*cis*-C	H	H	*trans*-C
1-*cis*, 5-*cis*-dicaffeoylquinic acid	*cis*-C	H	H	*cis*-C
3-*trans*, 4-*trans*-dicaffeoylquinic acid	H	*trans*-C	*trans*-C	H
3-*trans*, 4-*cis*-dicaffeoylquinic acid	H	*trans*-C	*cis*-C	H
3-*cis*, 4-*trans*-dicaffeoylquinic acid	H	*cis*-C	*trans*-C	H
3-*cis*, 4-*cis*-dicaffeoylquinic acid	H	*cis*-C	*cis*-C	H
3-*trans*,5-*trans*-dicaffeoylquinic acid	H	*trans*-C	H	*trans*-C
3-*trans*,5-*cis*-dicaffeoylquinic acid	H	*trans*-C	H	*cis*-C
3-*cis*,5-*trans*-dicaffeoylquinic acid	H	*cis*-C	H	*trans*-C
3-*cis*,5-*cis*-dicaffeoylquinic acid	H	*cis*-C	H	*cis*-C
4-*trans*,5-*trans*-dicaffeoylquinic acid	H	H	*trans*-C	*trans*-C
4-*trans*,5-*cis*-dicaffeoylquinic acid	H	H	*trans*-C	*cis*-C
4-*cis*,5-*trans*-dicaffeoylquinic acid	H	H	*cis*-C	*trans*-C
4-*cis*,5-*cis*-dicaffeoylquinic acid	H	H	*cis*-C	*cis*-C

Q = quinic acid; trans-c = trans-caffeic acid; cis-c = cis-caffeic acid

Scheme 1. Structures of the dicaffeoylquinic acid regioisomers.

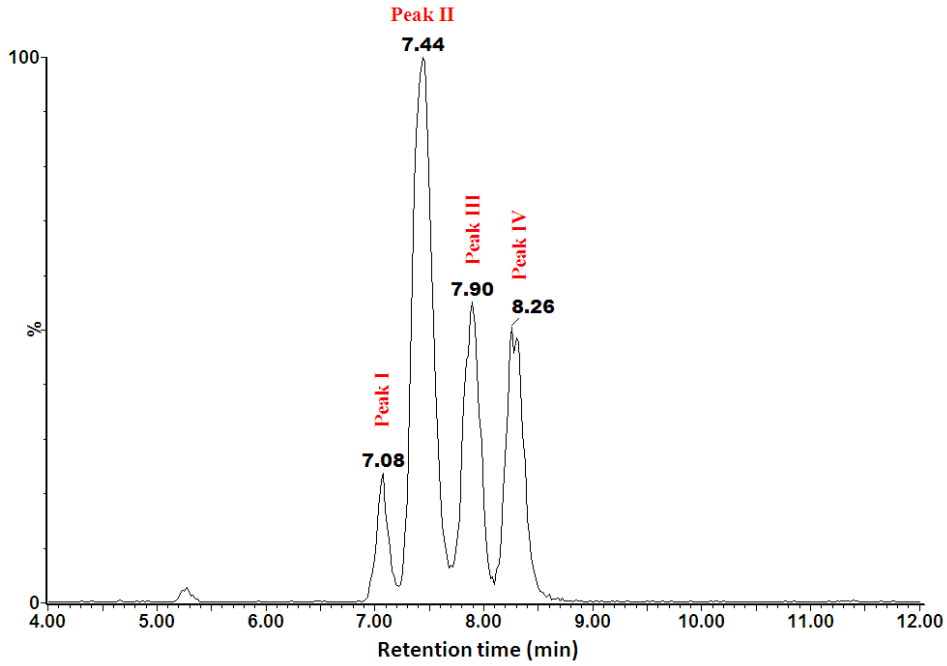

Figure 1. A representative UHPLC-Q-TOF-MS base peak intensity (BPI) chromatogram showing the separation of different geometrical isomers of 3,5-diCQA generated during UV exposure. Peak I: di-*cis* isomer, peak II: di-*trans*, peak III: mono-*cis* 1 and peak IV: mono-*cis* 2.

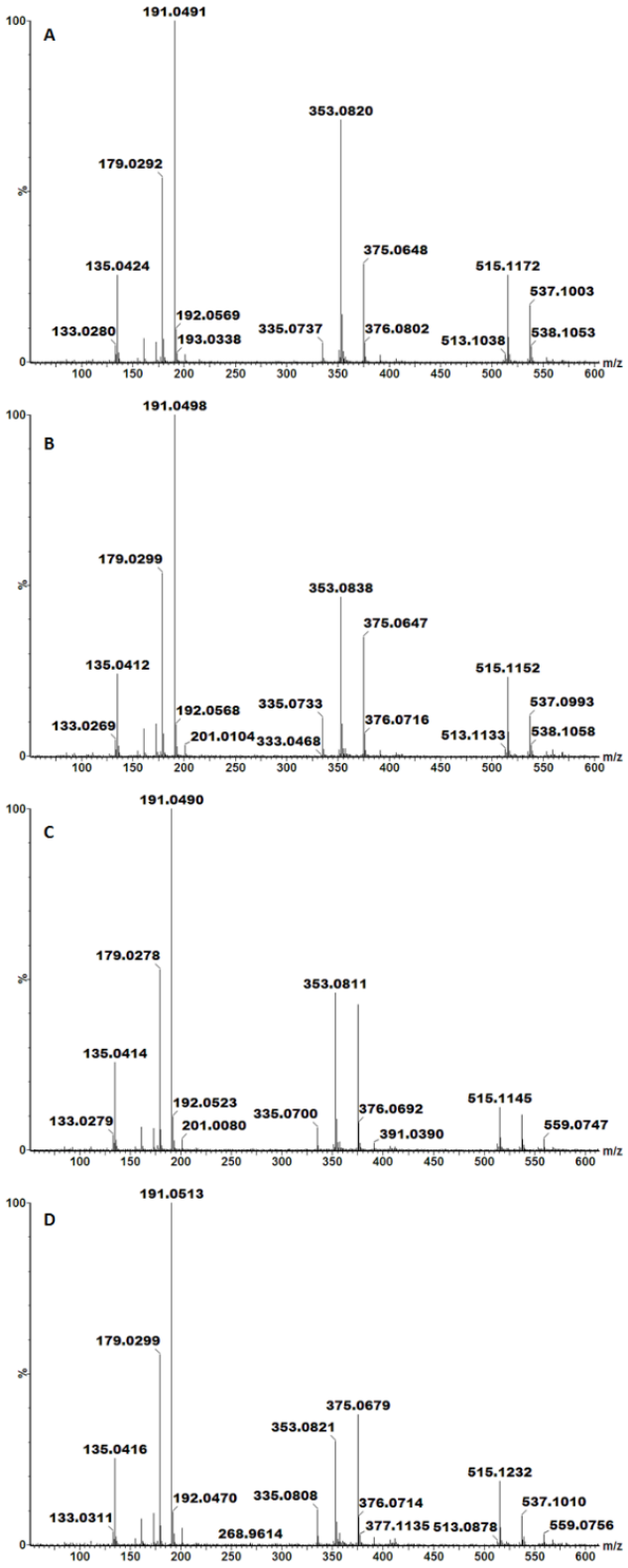

Figure 2. Representative Q-TOF-MS spectra for the (A) di-*trans*, (B) mono-*cis* 1, (C) mono-*cis* 2, and (D) *di-cis* geometrical isomers of 3,5-diCQA with the differentiating diagnostic sodium adduct $[M-2H-162+Na]^-$ peak seen at *m/z* 375.065. The data was collected at a capillary voltage 3.5 kV and cone voltage 60 V.

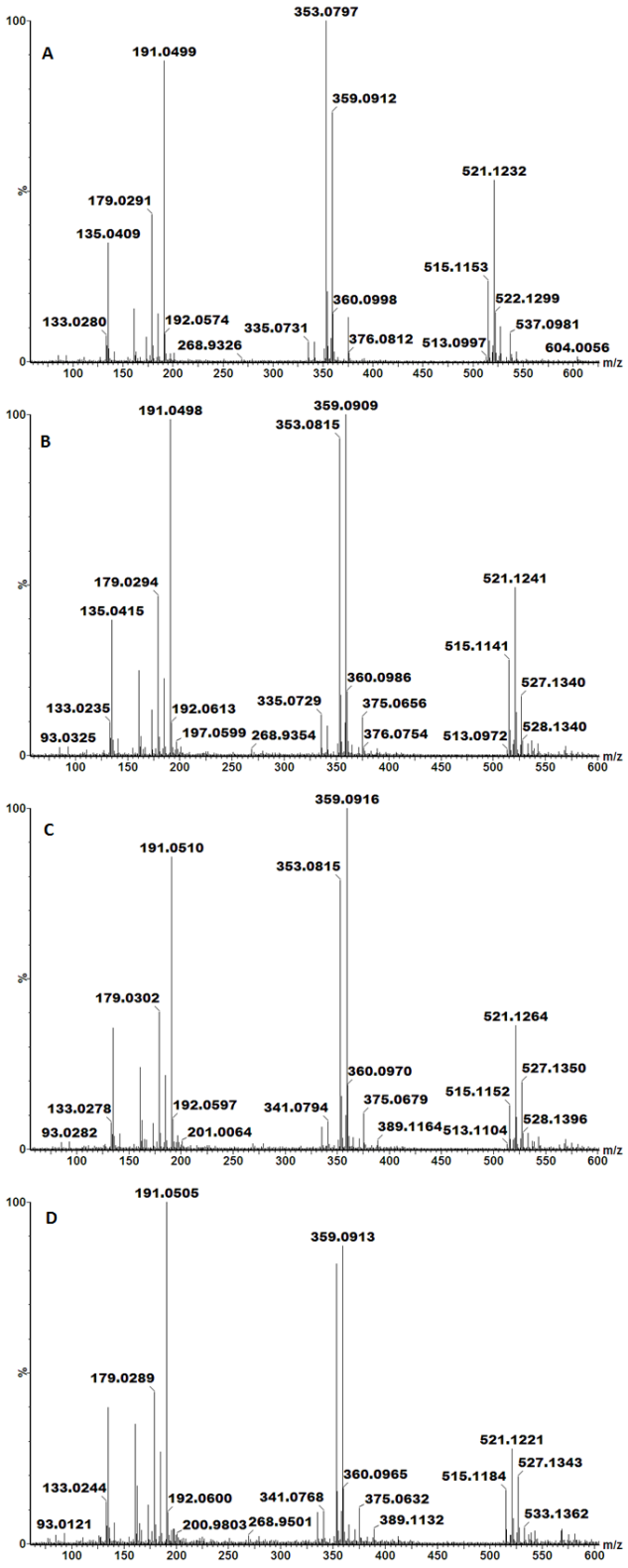

Figure 3. Representative Q-TOF-MS spectra for the (A) di-*trans*, (B) mono-*cis* 1, (C) mono-*cis* 2, and (D) di-*cis* geometrical isomers of 3,5-diCQA with the differentiating diagnostic lithium adduct $[M-2H-162+Li]^-$ peak seen at *m/z* 359.091. The data was collected at capillary voltage 3.5 kV and cone voltage 60 V.

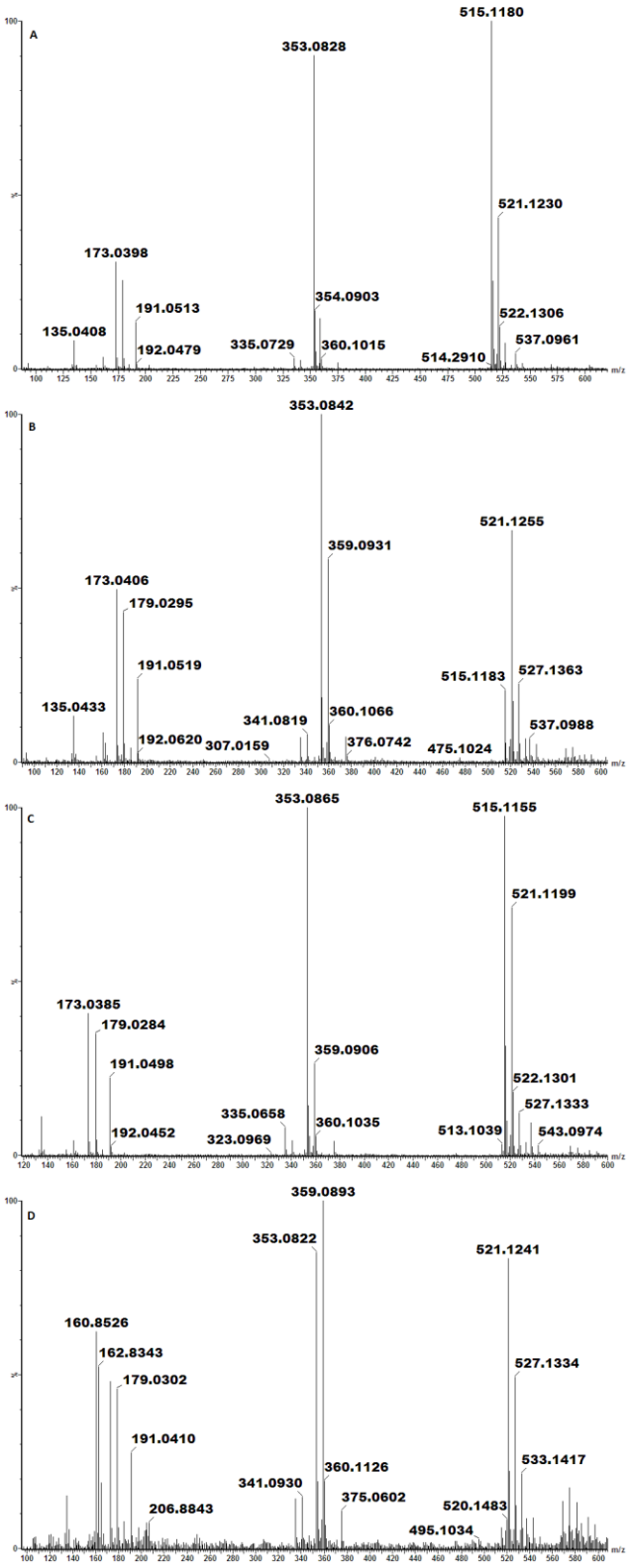

Figure 4: Representative Q-TOF-MS spectra for the (A) di-*trans*, (B) mono-*cis* 1, (C) mono-*cis* 2, and (D) *di-cis* geometrical isomers of 4,5-diCQA with the differentiating diagnostic lithium adduct $[M-2H-162+Li]^-$ peak seen at *m/z* 359.089. The data was collected at capillary voltage 3.5 kV and cone voltage 60 V.

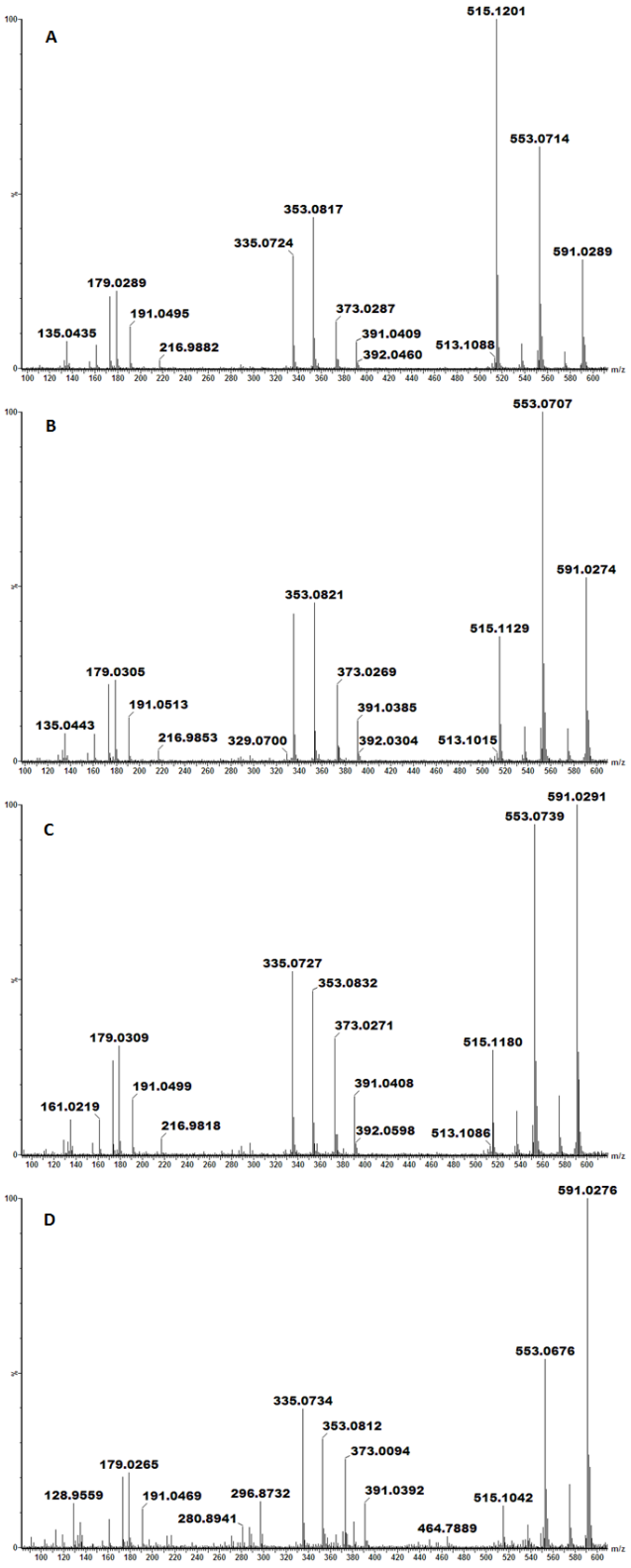

Figure 5: Representative Q-TOF-MS spectra for the (A) di-*trans*, (B) mono-*cis* 1, (C) mono-*cis* 2, and (D) *di-cis* geometrical isomers of 3,4-diCQA with the differentiating diagnostic potassium adduct $[M-3H+2K]^-$ peak seen at *m/z* 591.0276. The data was collected at capillary voltage 3.5 kV and cone voltage 60 V.